Biophysical Journal, Volume *117*

Supplemental Information

Simulation of Gating Currents of the *Shaker* K Channel Using a Brownian Model of the Voltage Sensor

Luigi Catacuzzeno and Fabio Franciolini

Supplemental Information

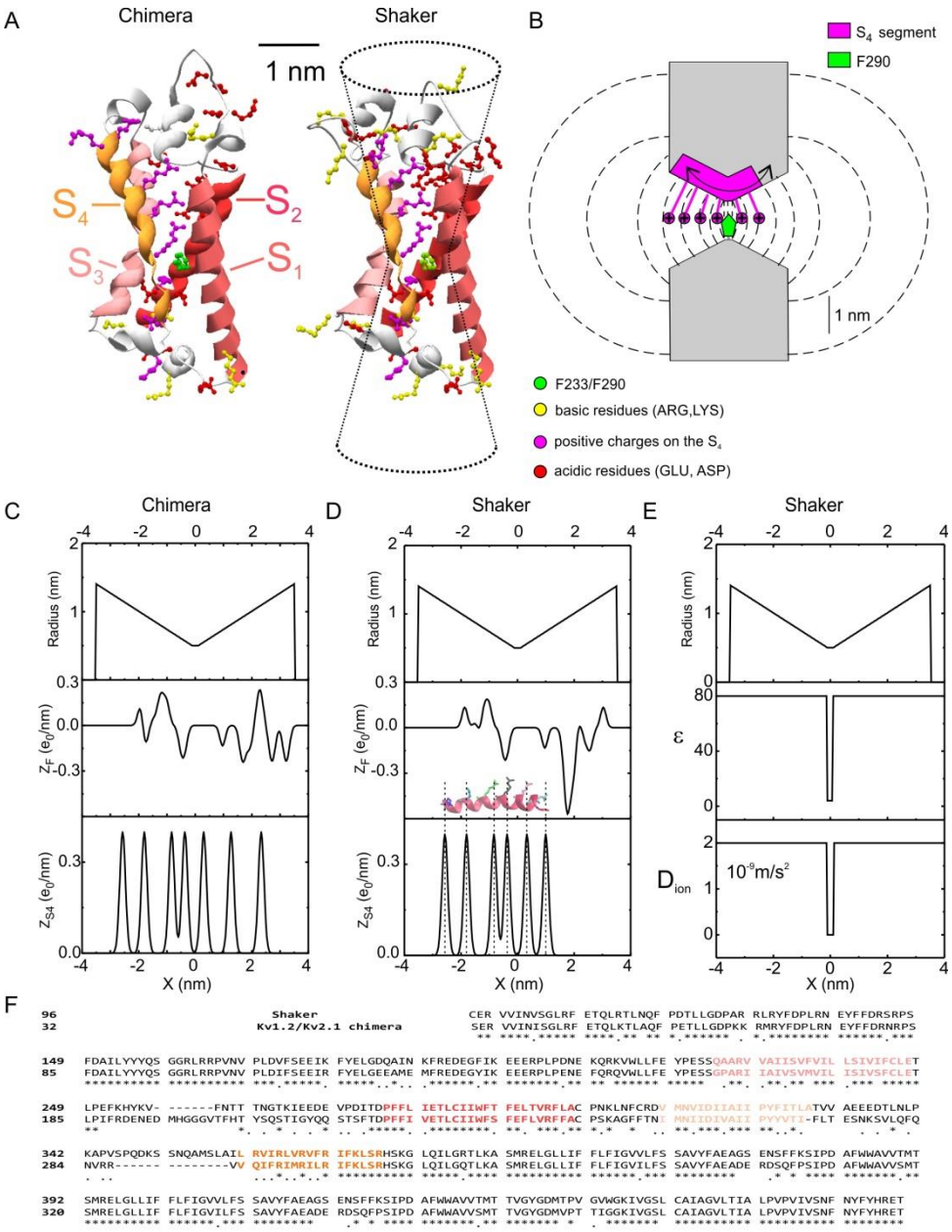

Supplementary Figure 1. A) Representation of one VSD from the Kv1.2/Kv2.1 chimera (structure 2R9R, left) in the activated state, and a model of the Shaker 3D structure obtained by homology modeling using the 2R9R structure as template (right). In both structures gating charges on the S_4 segment are in magenta, while negative and positive residues located in the remaining parts of the VSDs are in red and yellow, respectively. The residues F233 (in the chimera) and F290 (in Shaker) are in green. The hourglass-shaped drawing superimposed to the Shaker structure represents the geometry used in our model to delimit the gating pore and vestibules. The superimposition shows that the choice of 15° as half angle aperture approximates quite well the shape of the vestibules. **B**) Schematics showing the geometry of the VSD assumed in our model. The S_4 segment containing the 6 gating charges was assumed to move perpendicular to the membrane through the gating pore (0.2 nm long) and the extracellular and intracellular vestibules (each 3.4 nm long, and opening with a half angle of 15°). The dashed lines represent some of the surfaces delimiting the volume elements considered in our numerical simulations (see text for details). **C)** and **D)** Profiles of the gating pore radius, the fixed charge density located in the S1-S3 region of the VSD (Z_F), and the charge density on the S_4 segment (Z_{S4}) , for the Kv1.2/Kv2.1 chimera (left) and the Shaker model structure (right). For symmetrical reasons, x=0 was assumed to coincide with the center of the gating pore, where the F233/F290 residue is assumed to be located. *Inset:* 3D structure of the S_4 segment region of the Shaker channel model, with the R1-R6 charged residues explicitly shown in liquor ice representation. Notice the reasonable correspondence between the peaks of the Z_{S4} profile and the charged atoms of the R1-R6 residues. **E)** Profiles of the gating pore radius, the relative dielectric constant (ε) and the electrolyte ion diffusion coefficients (D_{ion}) as a function of the spatial coordinate considered in our model (x). **F)** Sequence alignment for the Kv1.2/Kv2.1 chimera and the Shaker K channels. * indicates conserved residues, while . indicates residues with similar polarity.

Validation of the steady-state approximation for ion dynamics in the solution of the Fokker-Planck equation

In order to numerically find the probability density function of the S_4 segment's position it is necessary to make an approximation in our model, consisting in the assumption that the electrolyte ions equilibrates instantaneously (cf. above). This steady-state approximation is very reasonable, since electrolyte ions move at a rate much faster than the movement of the S_4 segment. We however verified its validity by comparing the output of the full model used in the simulation of the single S_4 segment dynamics with that of a reduced model containing the described approximation. In the Supplementary Figure 2A we compared the amplitude histograms of the S4 segment positions built from simulations obtained with the full model – that is, the amplitude histograms already shown in Figure 2B of the paper – with the amplitude histograms obtained from simulations done using the reduced model, represented by the superimposed red lines.

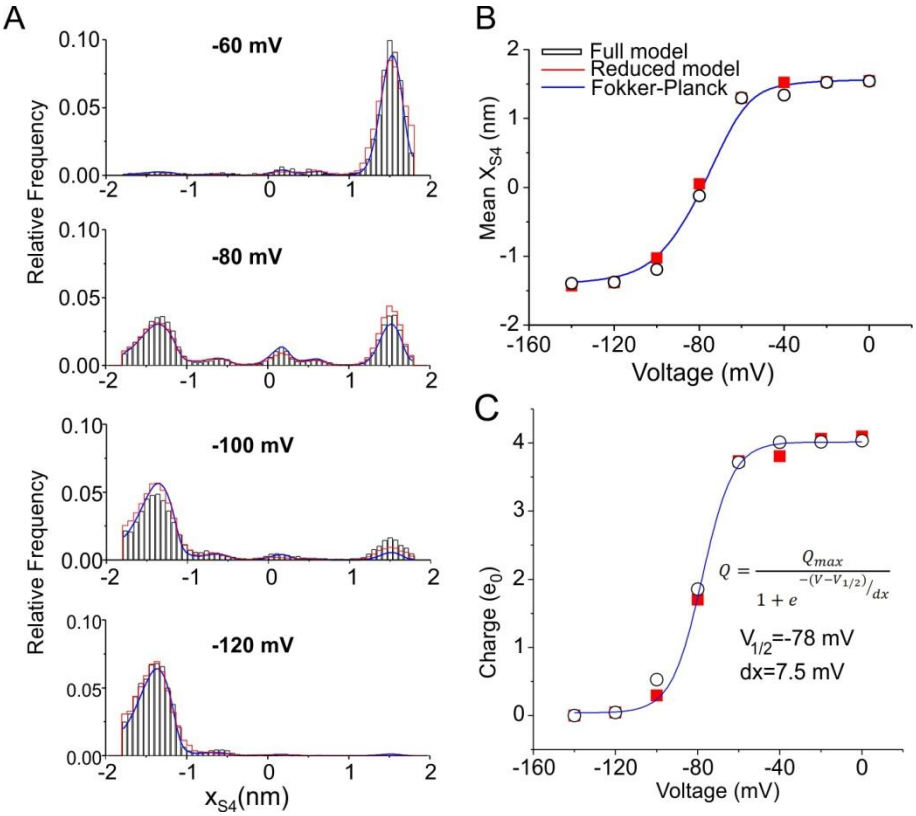

Supplementary Figure 2. A) Amplitude histograms of the S_4 segment position x_{S4}, obtained from 100 ms simulations at the indicated voltages. The black columns are simulation obtained with the full model, also shown in Figure 2 of the Ms. The red lines represent amplitude histograms obtained by running stochastic simulations of the reduced model, assuming instantaneous steady-state for the electrolyte ion concentrations. The blue lines represent the probability density function of the S_4 segment position, found by solving the FP equation up to equilibrium, at the four different applied voltages. **B)** Plot of the mean x_{S4} as a function of the applied voltage, assessed using the full stochastic (circles, also reported in Figure 2C of the Ms), the reduced stochastic (red squares) and the FP (blue line) models. **C)** Plot of the mean charge vs the applied voltage, obtained by integrating the microscopic gating current over 50 ms long simulations at different applied voltages. The simulations used are the same reported in Figure 5 on the Ms. black and red symbols refer to simulations performed using the full or the reduced model, respectively. The solid blue line represents the fit of the full model data with a Boltzmann relationship, with best fit parameters indicated in the Figure.

The blue lines in the same Figure represent instead the predicted probability density function of the S_4 segment position, obtained by solving the FP equation, thus also including the above mentioned approximation. It is

evident that the differences between the curves derived from the full and the reduced models are within the variability originating from the stochastic nature of the simulations, thus validating the approximation. In Supplementary Figure 2B we plot the mean S_4 position vs voltage assessed for the full model (data already shown in Figure 2C of the Ms) and compared it with that obtained by using either single particle simulations obtained from a reduced model or by directly solving the FP equation. Also in this case a full agreement was obtained. Finally, we also compared the full and reduced models in predicting the behavior of the gating currents originating from the movement of a single S_4 segment. As shown in Supplementary Figure 2C, the voltage dependence of the mean charge displacement assessed from the time integral of the gating currents results very similar between the two models, again validating the steady-state approximation for electrolyte ions electro-diffusion.

Macroscopic gating currents after subtraction of the linear component

Supplementary Figure 3A shows a simulation of the macroscopic gating current obtained in response to a membrane depolarization from -140 to -40 mV (and with the tested assumption that the electrolyte ions equilibrate instantaneously). Several features of the simulated response have been also observed in experiments. First, within the few microseconds after the beginning of the depolarizing step a very fast gating current component appears, raising instantaneously and then falling very rapidly (*cf.* inset to Figure 3A). This fast component has been experimentally observed using high speed recordings (43). Second, the fast gating current component is followed by a slower component starting with a plateau/rising phase and continuing with a slow decay Figure 7A, main). The plateau phase disappears at small depolarizations, while it becomes a prominent rising phase for larger depolarizations (cf. Figure 7A and C, main). All these features of the macroscopic gating currents have been observed experimentally (3).

In real experiments gating currents are isolated from other types of (linear) capacitive components by standard subtracting protocols (i.e., the currents obtained in response to a depolarizing pulse in a voltage range where the response is no longer voltage-dependent are subtracted from the gating current recorded in the voltage range activating the gating structures). Following this experimental procedure, we simulated the response to a 100 mV depolarization applied from a holding voltage of -300 mV, well outside the activation range of the voltage sensor. As shown in Figure 3B this voltage step evoked only very fast currents resembling the fast component of the gating current shown in panel A. However, the subtraction procedure, shown in Figure 3C, did not completely eliminate the fast component from the macroscopic gating current, indicating that it is not a fully linear component, but a specific feature of the gating current that originates in part from the movement of the gating charges along the activation pathway.

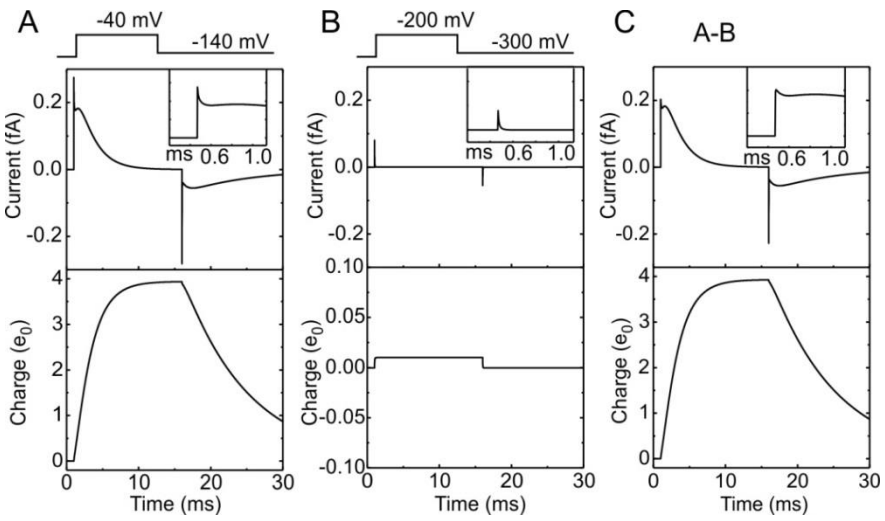

Supplementary Figure 3. A) The upper panel shows a simulated macroscopic gating current evoked by a voltage pulse from -140 to -40 mV (protocol indicated above). The inset is a time expansion of the fast gating current component present at the beginning of the depolarization. The lower panel represents the time integral of the gating current, expressed in units of unitary charges (e0). **B)** Simulated gating currents evoked using a voltage pulse from -300 to -200 mV, to verify whether a fast component of the gating current can be evoked outside the voltage range for S_4 segment movement among different states. **C)** Traces obtained from the subtraction of the time course in B from those shown in A, to simulate a leak subtraction as performed in experiments.

Addition of a spring-type force acting on the S_4 segment

As shown in the main text of the Ms, our model predicts a Q-V relationship moved 20/30 mV towards the hyperpolarizing direction as compared to that observed in experiments. A possible reason for this discrepancy is suggested by experiments showing that mutations that functionally uncouple the voltage sensor from pore opening tend to move leftwards the Q-V relationship, indicating that in a real channel the pore domain exerts on the voltage sensor a force discouraging its activation. Since our model does not contain any pore domain, the more hyperpolarized Q-V relationship is simply expected. In order to verify this hypothesis, we added to our model a spring-type force acting on the voltage sensor (Supplementary Figure 4A), and looked at the resulting gating currents and I-V relationship. More specifically the force acting on the voltage sensor, that in our model was exclusively electrical in origin (eqn. 7 in Material and Methods), was modified so as to include a term representing a Hook spring:

$$F_{ex}(x_{S4}, t) = -e_0 \int Z_{mS4}(\epsilon) \left(\frac{dV(\epsilon,\ t)}{d\epsilon} \right) d\epsilon + k_{sp}\ (x_{S4} - x_{eq})$$

where k_{sp} is the spring constant and x_{eq} is the equilibrium position of the spring, assumed to be coincident with the resting state of the voltage sensor ($x_{eq} = -1.33\ nm$).

As shown in Supplementary Figure 4B and C, inclusion of a spring-type force moved the Q-V relationship towards more depolarized voltage, without affecting the main kinetic properties of the gating

current. Thus inclusion of a pore domain "weighting" on the S_4 segment may recover the voltage-dependence of the Q-V relationship found experimentally.

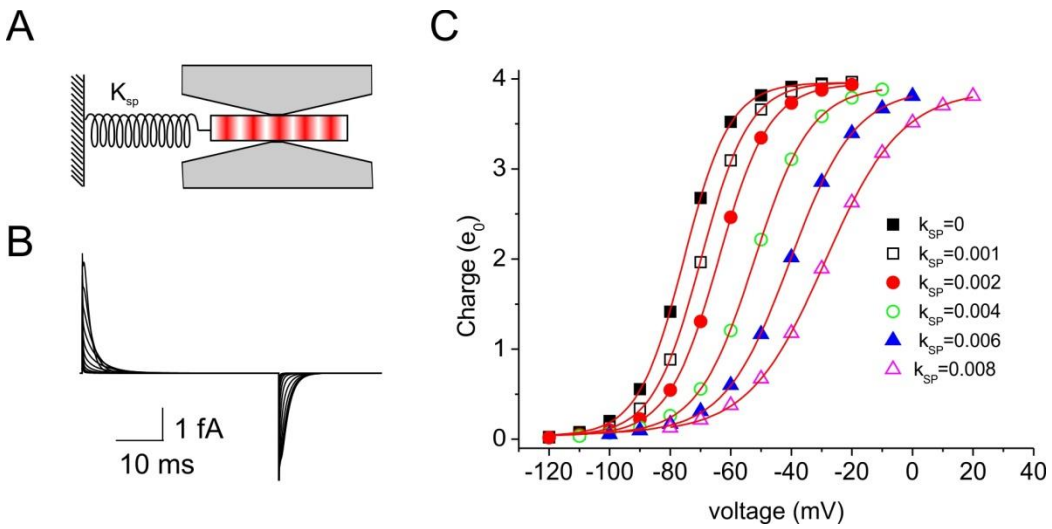

Supplementary Figure 4. A) Schematic drawing illustrating a spring that exerts a force that tends to keep the S_4 segment in its resting position. **B)** Family of simulated gating currents obtained in response to depolarizing steps from -100 to 0 mV, from a holding potential of -140 mV, obtained using a model including a spring with parameters k_{sp}=0.006 N/m and x_{eq}=-1.33 nm contributing to the force acting on the voltage sensor. **C)** Plot showing the effect of including a spring having different k_{sp} (indicated; in N/m) on the predicted Q-V relationship.

Validation of the model: conservation of the total current

We validated our model by verifying that the total current produced was conserved along the spatial domain. It has been recently shown that the application of the Maxwell equations to models involving the movement of charges gives rise to a very simple rule that applies independently to the details of the model and the time scale considered: the current produced by moving masses, when summed up to a displacement current, proportional to the temporal changes in the electric field, results in a total current that should remain constant in space (46,47).

Although our model for the macroscopic gating current considers a population of S_4 segments, we first consider only one S_4 segment inside its voltage sensor domain and surrounded by K and Cl ions in the baths and vestibules. For this system a current conservation can be written for each type of moving charge of the system

$$\frac{d\rho_j(x,t)}{dt} = -\frac{d(i_j(x,t)/A(x))}{dx} \quad \text{(S1)}$$

where $\rho_j(x,t)$ is the charge density (charge per unit volume) of species j (in our model either monovalent anion and cation, or the charged S_4 segment), t is the time, and i_j is the current produced by species j (charge per unit time), and $A(x)$ is the surface normal to the particle flux. Summing up the current conservation equations for all species we obtain:

$$\frac{d\rho(x,t)}{dt} = -\frac{di(x,t)/A(x)}{dx} \quad \text{(S2)}$$

With $\rho(x,t) = \sum \rho_{ions}(x,t) + \rho_{S4}(x,t)$ being the total moving charge density, and $i(x,t) = i_{ions}(x,t) + i_{S4}(x,t)$ being the particle current.

In our model $i_{ions}(x,t)$ is assessed on the assumption that ions cannot pass through the gating pore, and by applying charge conservation. More specifically:

$$i_{ions}(x,t) = \frac{d}{dt}\int_x^{x_{pl}} A(x)\, F\, \left(\sum_{j=0}^{nions-1} c_j(x,t) z_j\right) dx = -\frac{d}{dt}\int_{x_{pr}}^{x} A(x)\, F\, \left(\sum_{j=0}^{nions-1} c_j(x,t) z_j\right)\ dx \quad \text{(S3)}$$

Where x_{pl} and x_{pr} are the left and right extremes of the gating pore, F is the Faraday constant, and z_j is the valence of ion j. From similar considerations, $i_{S4}(x,t)$ can be assessed as

$$i_{S4}(x,t) = \frac{d}{dt}\int_x^L e_0\, z_{mS4}(x,t)\ \ dx = -\frac{d}{dt}\int_0^x e_0\, z_{mS4}(x,t)\ \ dx \quad \text{(S4)}$$

Where $z_{S4}(x,t)$ is the valence density profile of the S_4 segment.

Finally, in our model all the charges contribute to shape the electric field E in accordance with the Gauss law, that in the differential and mono-dimensional form reads

$$\varepsilon_0\ \frac{d[A(x)\ \varepsilon(x)\ E(x,x_4,t)]}{dx}\ = \rho^*(x,t) \quad \text{(S5)}$$

Where $\rho^*(x,t) = \sum \rho_{ions}(x,t) + \rho_{S4}(x,t)\ + \rho_F$, with ρ_F being the time- and position-independent fixed charge, and $E(x,x_4,t)$ is the electric field, for which we have explicitly indicated the dependence on the spatial dimension, time, and position of the voltage sensor x_{S4}. Taking the time derivative of eqn. (S5) we obtain

$$\varepsilon_0\ \frac{d}{dx}\left[A(x)\ \varepsilon(x)\frac{dE(x,x_4,t)}{dt}\right]\ = \frac{d\rho^*(x,t)}{dt} = \frac{d\rho(x,t)}{dt} \quad \text{(S6)}$$

And combining eqns (S2) and (S6) we obtain

$$\frac{d}{dx}[i_{tot}(x,t)] = 0 \quad \text{(S7)}$$

which shows the conservation of the total current defined as:

$$i_{tot}(x,t) = i_{ions}(x,t) + i_{S4}(x,t) + i_{displ}(x,t) \quad \text{(S8)}$$

where we have introduced the displacement current

$$I_{displ}(x,t) = A(x)\ \varepsilon_0\ \varepsilon(x)\frac{dE(x,x_4,t)}{dt} \tag{S9}$$

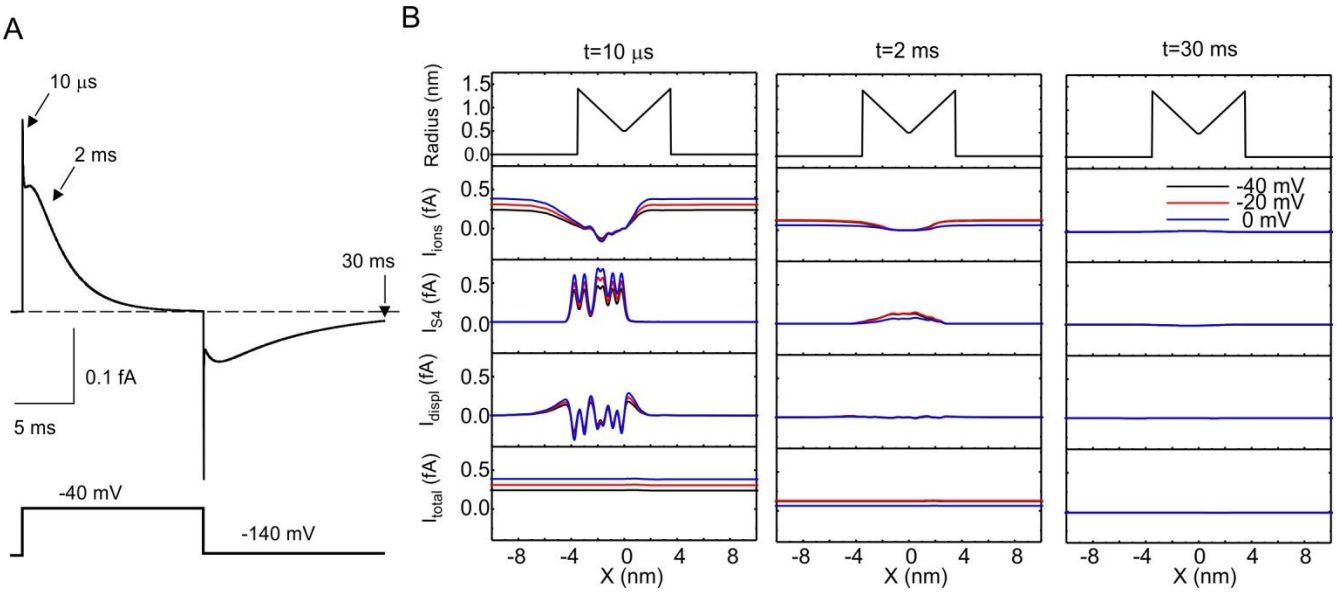

Supplementary Figure 5. A) Simulated macroscopic gating current evoked by a voltage pulse from -140 to -40 mV (protocol indicated below). **B)** Plots of the vestibules and gating pore radius (Radius), the ionic current (I_{ions}), the S_4 segment (I_{S4}) and displacement (I_{displ}) currents, and total current (I_{total}) as a function of the spatial dimension (x), at three different times from the beginning of the depolarization and three different depolarizing voltages (indicated).

In our model we actually consider a population of S_4 segments, distributed in the allowed positions x_{S4} in accordance with the density function $f_{S4}(x_4, t)$, assessed by solving the Fokker Planck equation. In order to find a conservation equation to apply to the mean macroscopic gating current, we integrate eqn. (S6) for all possible positions of the S_4 segment, weighting with the density function $f_{S4}(x_4, t)$.

$$\int_{-x_L/2}^{x_L/2}\frac{d}{dx}\left[A(x)\ \varepsilon_0\varepsilon(x)\frac{dE(x,x_4,t)}{dt} + i(x,t)\right] f_{S4}(x_{S4})\ dx_{S4} = 0 \tag{S10}$$

Where $\pm x_L/2$ represent the extreme positions allowed to the S_4 segment. Rearranging

$$\frac{d}{dx}[I_{displ}(x,t) + I_{ions}(x,t) + I_{S4}(x,t)] = 0 \quad \text{(S11)}$$

Where

$$I_{displ}(x,t) = \frac{d}{dt}\int_{-x_L/2}^{x_L/2}[A(x)\,\varepsilon_0\varepsilon(x)E(x,x_4,t)]\,f_{S4}(x_{S4})\,dx_{S4} \quad \text{(S12)}$$

$$I_{ions}(x,t) = \int_{-x_L/2}^{x_L/2} i(x,t)\,f_{S4}(x_{S4})\,dx_{S4} = \frac{d}{dt}\int_{-x_L/2}^{x_L/2}\left[\int_x^{x_{pl}} A(x)\,F\left(\sum_{j=0}^{nions-1} c_j(x,t)z_j\right)\right] f_{S4}(x_{S4})\,dx_{S4} \quad \text{(S13)}$$

$$I_{S4}(x,t) = \frac{d}{dt}\int_{-x_L/2}^{x_L/2}\left[\int_x^{L} e_0\,z_{S4}(x,x_{S4})\;\;dx\right]\,f_{S4}(x_{S4})\,dx_{S4} \quad \text{(S14)}$$

Supplementary Figure 5 shows the total current profile, together with the three contributing currents (ionic, S_4 segment, and displacement currents), assessed using eqns (S12), (S13) and (S14) at three different times (10μs, 2 ms,and 30 ms) from the beginning of a depolarizing pulse from -140 to three different test voltages (indicated). As expected the conservation of the total current is respected in all regions considered (baths, channel vestibules and gating pore), and under different conditions.

Sensitivity analysis

We performed a sensitivity analysis to show how robust are the model results presented above upon varying the main parameters used in the model. Supplementary Figure 6A shows that the friction coefficient of the S_4 segment controls the rate of the ON and OFF gating currents. From a qualitative point of view, however, the gating currents obtained using different γ values are not very different, with the various kinetically distinct phases remaining evident for all γ's. In addition changing γ does not significantly affect the Q-V relationship (panel C). Altogether these results indicate that the quantitative value of this parameter does not affect the potential of our model to reproduce the main qualitative properties of the gating currents, such as the presence of the two different components.

Supplementary Figure 6B-E shows the effect of varying the structural dimensions of the gating pore (length l and diameter d), the standard deviation of the normal distribution used to spread each protein charge considered (σ) and the dielectric constant within the gating pore (ε). In general, all these parameters affected the rate of the gating currents much more that the steady state Q-V relationship, suggesting that the properties of the gating pore are important in setting the rate of the voltage sensor movement, while the fixed charge distribution, but not its exact shape, is more important for setting the equilibrium position of the voltage sensor.

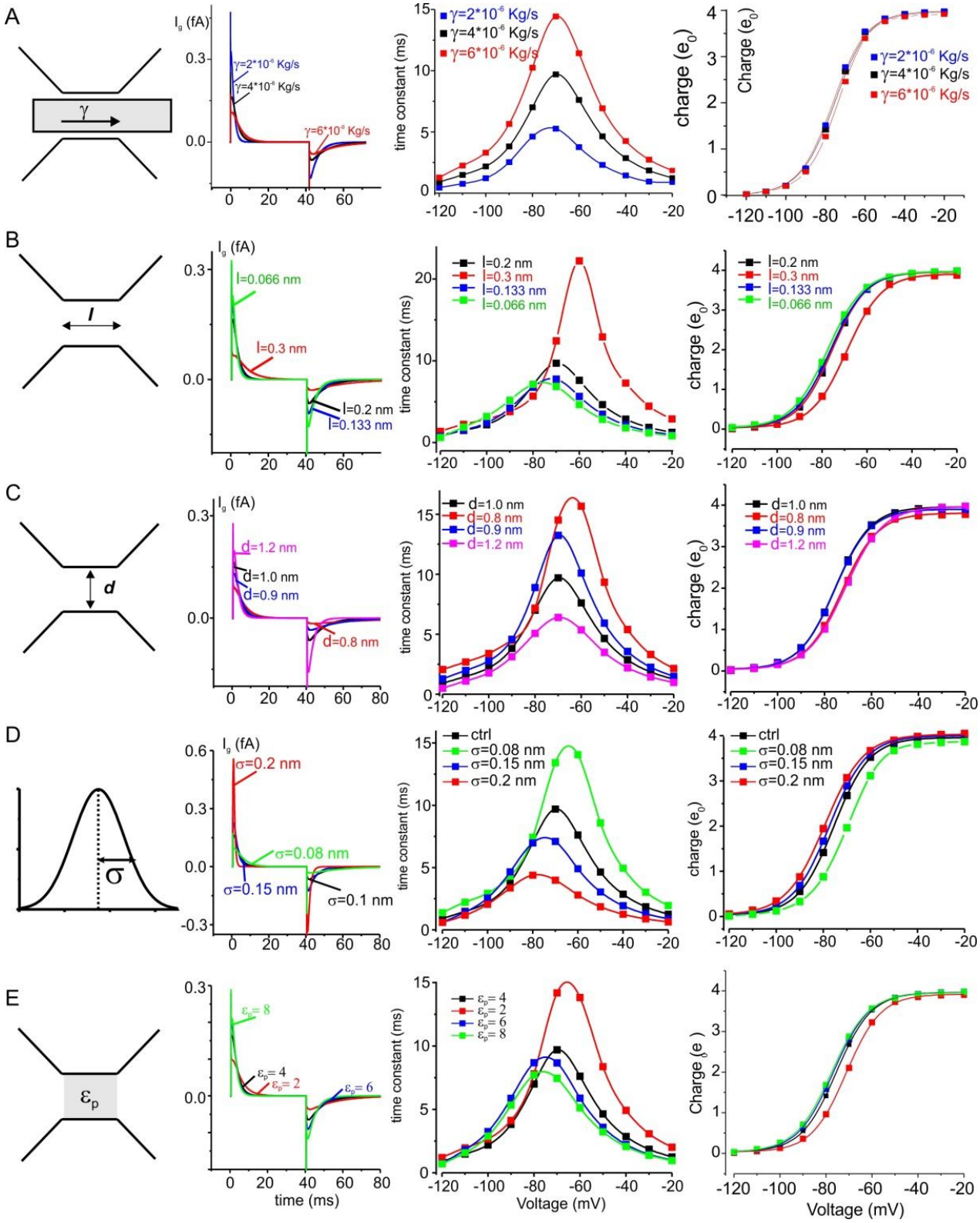

Supplementary Figure 6. Simulated macroscopic gating currents, time constant vs voltage relationships, and Q-V relationships obtained with our model while varying the indicated parameter.